Regular article

The transition from linear to-parabolic growth of Cu$_3$Si phase in Cu/a-Si system

Bence Parditka [a], Hanaa Zaka [a,b], Gábor Erdélyi [a], Gábor A. Langer [a], Mohammed Ibrahim [c], Guido Schmitz [d], Zoltán Balogh-Michels [e,*], Zoltán Erdélyi [a]

[a] Department of Solid State Physics, University of Debrecen, P.O. Box 400, H-4002 Debrecen, Hungary
[b] Nano-Science & Semiconductor Laboratories, Department of Physics, Faculty of Education, Ain Shams University, Cairo 11566, Egypt
[c] Physics Department, Faculty of Science and Art, Al Jouf University, Al-Qurayyat, Saudi Arabia
[d] Institute of Materials Science, University of Stuttgart, Heisenbergstraße 3, D-70569 Stuttgart, Germany
[e] Center of X-Ray Analytics, Empa, Swiss Federal Laboratories for Materials Science and Technology, Überlandstrasse 129, CH8600 Dübendorf, Switzerland

ARTICLE INFO

ABSTRACT

The solid state reaction between Cu and a-Si films was investigated at 150–200 °C by depth profiling with secondary neutral mass spectrometry. Intermixing was observed leading to the formation of a homogeneous Cu$_3$Si layer at the interface. The growth of the crystalline silicide follows a parabolic law at 165 °C and 200 °C. At 150 °C a transition from linear to parabolic kinetics is observed. Combining with our previous experimental results showing linear kinetics at 135 °C [Acta Materialia, 61 (2013) 7173–7179], the temperature dependence of the linear and parabolic coefficients as well as the transition length can be estimated.
© 2018 Acta Materialia Inc. Published by Elsevier Ltd. This is an open access article under the CC BY-NC-ND license (http://creativecommons.org/licenses/by-nc-nd/4.0/).

Currently about 99% of all semiconductor devices are made from silicon [1]. The dominant material used in photovoltaic industry is also multi-crystalline silicon [2,3]. Polycrystalline Si is compromise between price and efficiency, i.e. it is cheaper than monocrystalline Si, but more efficient than amorphous Si [4–6]. It was found that metals in contact with amorphous silicon strongly reduce the crystallization time and temperature. This process is called metal-induced crystallization (MIC) [7,8]. It allows the crystallization of the amorphous Si thin films–typically a product of physical vapor deposition–at reduced temperatures. From a fundamental point of view, the case where the bond weakening of the a-Si is achieved by a solid state reaction is especially interesting (e.g. Ni in Ref [9] or Cu in Ref [10]).

Most of our theoretical knowledge about metal silicon reactions stems from the experiments having applications in microelectronics in mind, i.e. a thin metal layer reacted with a semi-infinite, single crystalline Si wafer. Ref [11] is an old but still very useful review concerning this context. One of the key statements in this review was that metal-silicon reactions are diffusion controlled. Nucleation is almost always easy (with some refractory

metals as the sole exceptions [12]) and linear growth kinetics is likely to be due to improper specimen preparation rather than reflecting the real physics of the given metal-silicon systems.

The investigation of different specimen geometries, especially thin layer interdiffusion couples/multilayers started to question the generality of these rules. New examples of linear kinetics were found in carefully prepared specimens [13–16]. Upon reviewing older literature (e.g. [17].) other precedents of deviations from the parabolic kinetics can be found, even if they were neglected in the original publications.

Similarly, it was also shown that nucleation can indeed play an important role [18–20] and it was the high diffusivity of transition metals in Si [21,22] and the surfactant property of Si [23] which ensured the easy nucleation environment.

Cu is an important material in the microelectronics as it is the most typical contact and heat sink material. Here, the goal is to prevent the formation of Cu$_3$Si [20,31]. But there are alternative applications in which the growth of Cu$_3$Si is desired. It was shown that the Cu-induced crystallization of amorphous Si proceeds with the aid of Cu$_3$Si phase [10,32]. Similarly for Li ion batteries, Si nanowires and nanorods as anodes have higher specific capacity and larger surface areas than graphite anodes. This leads to higher energy density and faster charging–discharging. This rod geometry is, however, brittle. Previous investigations (e.g., Ref [33]) reported improved cyclic stability by adding a

* Corresponding author at: Center for X-ray Analytics, Empa Swiss Federal Laboratories for Materials Science, Überlandstrasse 129, CH-8600 Dübendorf, Switzerland.
E-mail addresses: parditka.bence@science.unideb.hu (B. Parditka), erdelyi@science.unideb.hu (G. Erdélyi), glanger@science.unideb.hu (G.A. Langer), guido.schmitz@mp.imw.uni-stuttgart.de (G. Schmitz), zoltan.balogh@empa.ch (Z. Balogh-Michels), zoltan.erdelyi@science.unideb.hu (Z. Erdélyi).

copper coating which forms Cu_3Si with the Si nanorods during the charging-discharging cycles.

In our previous investigations we have found that the growth of Cu_3Si in the Cu/a-Si is far from being a simple diffusion controlled case. If Cu is deposited on a-Si, fast nucleation of 10–20 nm Cu_3Si takes place even at very low temperature [16,18,19]. Dynamic segregation during deposition creates a thick mixed zone between Cu and a-Si. The thickness of this zone is enough to allow the rapid nucleation in polymorphic mode [24,25] which can be considered as practically instantaneous. Following this nucleation, linear growth was observed at 135 °C [16]. Yet, in another multilayer experiment, Chromik et al. reported simple parabolic growth for temperatures of 200 °C and above [26]. If both these experiments are correct, a transition from "peculiar" to "normal" growth modes should happen in the 135–200 °C temperature range. In this work, we are describing our results from growth kinetics experiment at 150, 165 and 200 °C. We also insert our previous 135 °C growth kinetics [16] in the new framework.

The Cu/Si system contains multiple silicide phases [27], with Cu_3Si or η as the most stable one. More about the thermodynamics of the Cu/a-Si system can be found in Ref. [18] based on the theoretical and experimental data of Refs [26,28–30]. In short, solubility at the Si side is practically nil, while rather high (10–20%) at the Cu-side.

The specimen preparation method was described in details in Ref. [16]. We prepared bilayer stacks of 120 nm thick a-Si layer followed by an 80 nm thick nanocrystalline Cu layer onto a Si(111) wafer by DC magnetron sputtering at ambient temperature in a vacuum of 10^{-7} mbar. Each set of samples contained 5 pieces of 3 mm × 3 mm. Two of them were kept as deposited, while the other three were annealed at 150–200 °C for various times. Annealing was carried out under high vacuum conditions.

Intensity-time profiles were measured by an INA-X, SPECS Secondary Neutral Mass Spectrometer (SNMS) which allows excellent depth resolution (<2 nm) [34]. The raw SNMS data were transformed into concentration-depth profiles, using the sensitivity factors of the elements and the depth profiles as determined by using an AMBIOUS XP-1 profilometer [16,35].

To determine the thickness of the silicide, we start with an overall depth profile. Two mass windows, belonging to Si (28 amu), Cu (63 amu) were utilized. The SNMS depth profile of the samples contains typically a plateau with intermediate concentrations (Fig. 1). Additional Si peaks at the Cu/Si and Cu_3Si/Si interfaces are caused by the change of sputtering conditions at the metal–semiconductor transition, which is a well-known artifact. Falling edges of the Cu signal indicate the position of the Cu/Cu_3Si and Cu_3Si/Si interfaces. Afterwards, in independent sputter runs, craters are bored till these two interfaces. The depths of the craters were measured by the profilometer several times and in

several scan directions to obtain accurate averaged depth values that define the thickness of the reaction product. Dashed lines in Fig. 1 mark the phase boundaries of the silicide phase, being in this example 49 nm spaced to each other. Statistical and systematic errors are in the range of a few nanometers.

Following the nucleation, we observed a linear growth at 135 °C [16]. Nevertheless, after sufficiently large reaction thickness, diffusion through the silicide must become the rate limiting factor, a transition towards a parabolic growth shall be observed. The relation between the layer thickness (w) and the time (t) may be described by the following formula [36–38]:

$$t = \frac{1}{k}(w - w_0) + \frac{1}{2D}(w^2 - w_0{}^2),\qquad(1)$$

w_0 represents the layer thickness at a given t_0; the kinetic coefficients k and D relate to the interface and to the diffusion transport, respectively. By assuming an initially nucleated layer (w_0), we can set the experiment start point to any time. As we have a limited amount of data points, we use in the following single parameter plots (w^2–t and w–t) instead of the complete linear-parabolic fitting.

Because of the quadratic term, the w^2 versus t plots are less sensitive to the deviations from parabolic growth in the case of thin layers (e.g. Ref. [17]). The quadratic form also means that errors of the thickness squared contain the total thickness of the layer

$$\delta(w^2) = 2w\delta w,\qquad(2)$$

(δw is the error of the layer thickness measurement.) Consequently, the data from later stage are overweighed as compared to those of the earlier stage. The reverse is true for the linear plots. Thus, the interpretation of the data depends on the plotting method Nevertheless, plotting both the w^2–t and the w–t relations, we may draw unequivocal conclusions about the growth kinetics.

Let us discuss the quantitative results on the growth kinetics of the silicide layer. Fig. 2a and b show the growth kinetics for 135 °C and 150 °C in the linear (thickness vs time) and in the parabolic (square of the thickness vs time) plots. The data for 135 °C are taken from our previous report, Ref. [16].

The dashed lines in the figures indicate the "nucleation thickness" i.e. the reaction thickness after the instantaneous nucleation event. A clear linear relation is observed for the 135 °C annealing experiments. The early stages seem linear for the 150 °C too. However the last data point demonstrates already a downward deviation from the linear tendency. This indicates that the bulk diffusion become slower than the transport through the interfaces.

The parabolic graph (Fig. 2b) tells a consistent story. The later stages can be described by the parabolic growth but not the earlier stages, for which the slope is significantly depressed. Obviously, a process slower than bulk diffusion controls the growth of the layer.

Fig. 2c shows the data at parabolic scales for 150 °C and 165 °C. For the 165 °C experiment, the diffusion controlled regime is clearly dominant, deviations are very small if present at all. Finally, the 165 °C and the 200 °C experiments are plotted in the parabolic scale in Fig. 2d. A clear diffusion controlled growth is observed for the 200 °C case, with slightly higher diffusion coefficient. Since the reaction layer thickness reaches >60 nm in this case, the influence of the fast nucleation is diminished (400 nm² as compared to 4000 nm²).

Fig. 3 shows the parabolic coefficients in comparison with the results of Chromik et al. [26]. Our growth rate coefficients are below their trendline with larger scatter, but the discrepancy is within the possible temperature differences. Our activation energy for the parabolic growth rate coefficient is 72 ± 15 kJ/mol, while it is 94 kJ/mol in Ref [26]. The agreement is reasonable between the two datasets. The activation energy of the linear coefficient was calculated from the experiments at 135 °C, 150 °C and 165 °C. Since there is no real linear part in the 165 °C case only a lower
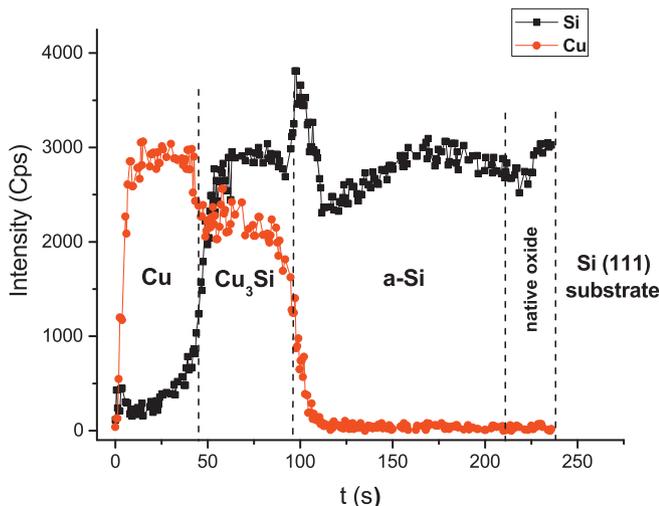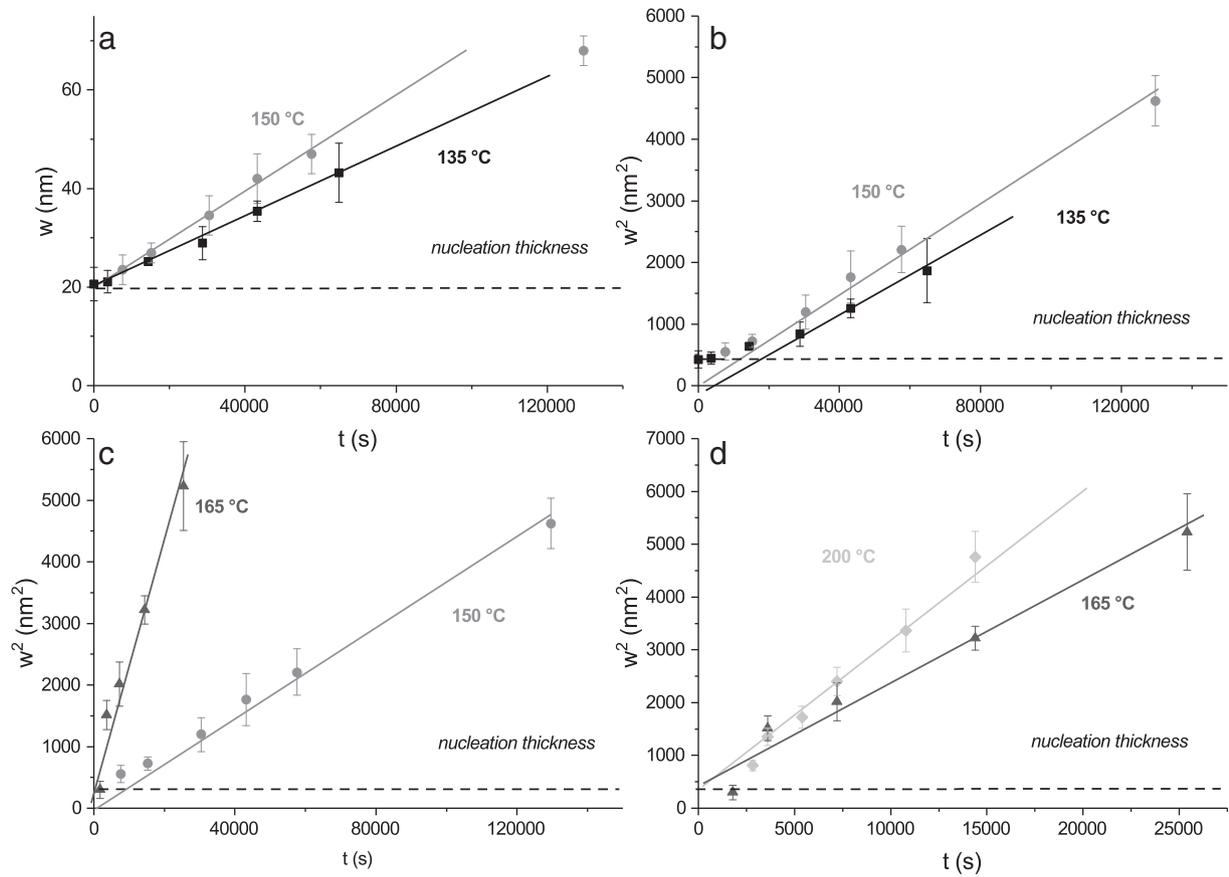

Fig. 1. Raw SNMS data of the specimen annealed at 200 °C for 2 h.

Fig. 2. Growth kinetics at 135 °C and 150 °C on the linear (a) and the parabolic (b) scale. Comparison of the kinetics at 150 °C and 165 °C (c) and 165 °C and 200 °C (d) on the parabolic scale. At low temperatures the linear kinetics offers a better description, but above 165 °C the deviations from the parabolic growth vanishes. The dashed line indicates the approximate thickness of the phase after the nucleation stage.

limit could be given, which amounts to 128 ± 50 kJ/mol. The fact that the barrier becomes more significant at low temperatures requires the higher activation energy for this coefficient. Apart from the temperature dependence of the parabolic growth rate coefficients, the product $0.5\,k \times w$ is also plotted in Fig. 3 for 10, 20, 50 and 100 nm thick layers. The crossing

of the parabolic and the linear growth rate coefficients marks the transition temperature for a given layer thickness. Or in a reverse way, the transition length at a given temperature can be estimated.

Table 1 summarizes the parabolic and linear coefficients. The transition length from linear to parabolic kinetics is estimated by fitting an Arrhenius function to the experimental data. For purely linear or parabolic growth, only the lower limits of the respective other coefficient can be given.

These data indicate that at low temperatures (<150 °C) there are three stages of the growth of the Cu_3Si. First, a fast transformation of the amorphous mixed layer [18,19] and the neighboring regions takes place, leading to a Cu_3Si layer of 10–20 nm thickness. At these low temperatures, the atomic jumps across the interface are hindered significantly [38]. This leads to an interface-controlled linear growth regime until a relatively large thickness of the silicide is reached. After that point, the silicide continues to thicken according to a parabolic law.

For high temperature (>150 °C) annealing, the transition length is comparatively short and the growth rates are higher. This means that for these annealing treatments neither the influence of the linear stage nor the initial thickness of nucleation is observable. Thus, unless high sensitivity in-situ experiments are used, no significant deviations from
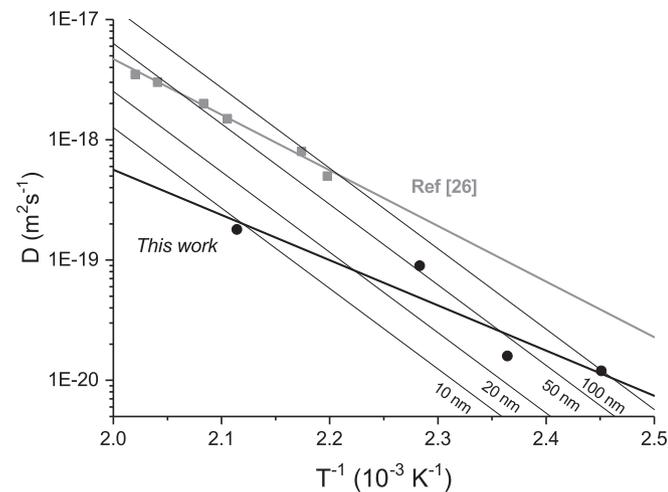
Fig. 3. Summary of the parabolic growth rate coefficients in comparison with the literature. Gray squares represent the data from Ref [26], black circles are the coefficients from this work, while thick lines are the respective fits. The thin lines represent $0.5\,k \cdot w$ for thicknesses, w as labeled. The effective transition temperatures are marked by the crossing of the thin lines with the Arrhenius representation of the diffusivity.

Table 1
Summary of the growth rate coefficients and the calculated transition length.

Temperature (°C)	2D ($m^2\,s^{-1}$)	k ($m\,s^{-1}$)	Trans. length (nm)
135	$<2.6 \times 10^{-20}$	3.4×10^{-13}	100
150	3.3×10^{-20}	5.3×10^{-13}	50
165	1.7×10^{-19}	$<4.6 \times 10^{-12}$	30
200	3.6×10^{-19}	$<4.6 \times 10^{-12}$	10

the diffusion controlled parabolic growth will appear at these experimental temperatures.

As a summary, we obtained growth data for the Cu$_3$Si phase using SNMS at different annealing temperatures. At 200 °C and 165 °C the growth was parabolic, while at 150 °C a linear-parabolic growth type was found. Using our earlier data measured at 135 °C, where the growth was linear, we can get a complete qualitative and quantitative description.

In the qualitative view, at high temperatures the growth is controlled by the bulk diffusion through the growing silicide layer, while at low temperatures the growth contains three stages. Fast nucleation of about 20 nm silicide, followed by an interface barrier controlled stage and finally a transition to diffusion controlled mode.

Quantitatively, we derived the activation energy for the parabolic growth coefficient (72 ± 15 kJ/mol) and the linear growth coefficient (128 ± 50 kJ/mol). The parabolic growth coefficients and the activation energy of interdiffusion are comparable to the literature values. Since the activation energy of the interface barriers is higher, they become more effective at lower temperatures. This finding agrees with the theoretical concepts on interface barriers [38].

Acknowledgements

References

[1] W. Zulehner, Mater. Sci. Eng. B 73 (2000) 7–15.
[2] L. Zhang, A. Ciftja, Sol. Energy Mater. Sol. Cells 92 (2008) 1450–1461.
[3] B.S. Xakalashe, M. Tangstad, Chem. Technol. (2012) 32–37.
[4] D. Sarti, R. Einhaus, Sol. Energy Mater. Sol. Cells 72 (2002) 27–40.
[5] A. Goetzberger, C. Hebling, H.W. Schock, Mater. Sci. Eng. R 40 (2003) 1–46.
[6] J.P. Murray, G. Flamanz, C.J. Roos, Sol. Energy 80 (2006) 1349–1354.
[7] Z. Wang, L.P. Jeurgens, E.J. Mittemeijer, in: Z. Wang, L.P. Jeurgens, E.J. Mittemeijer (Eds.), Metal Induced Crystallization: Fundamentals and Application, Pan Stanford 2015, pp. 1–24.
[8] S. Herd, P. Chaudhari, M.H. Brodsky, J. Non-Cryst. Solids 7 (1972) 309–327.
[9] E.A. Guliants, W.A. Anderson, J. Appl. Phys. 89 (2001) 4648–4656.
[10] Y.C. Her, C.W. Chen, C.L. Wu, J. Appl. Phys. 99 (2006) 113512.
[11] F.M. d'Heurle, P. Gas, J. Mater. Res. 1 (1986) 205–221.
[12] C.S. Petersson, J.E.E. Baglin, J.J. Dempsey, F.M. d'Heurle, S.J. LaPlaca, J. Appl. Phys. 53 (1982) 4866–4883.
[13] F. Nemouchi, D. Mangelinck, C. Bergmann, P. Gas, U. Smith, Appl. Phys. Lett. 86 (2005), 041903.
[14] T.E. Schlesinger, R.C. Cammarata, S.M. Prokes, Appl. Phys. Lett. 59 (1991) 449–451.
[15] C. Cserháti, Z. Balogh, A. Csik, G.A. Langer, Z. Erdélyi, G. Glodán, G.L. Katona, D.L. Beke, I. Zizak, N. Darowski, E. Dudzik, R. Feyerheim, J. Appl. Phys. 104 (2008), 024311.
[16] B. Parditka, M. Verzhak, Z. Balogh, A. Csik, G.A. Langer, D.L. Beke, M. Ibrahim, G. Schmitz, Z. Erdélyi, Acta Mater. 61 (2013) 7173–7179.
[17] S. Petersson, R. Anderson, J. Baglin, J. Dempsey, W. Hammer, F. d'Heurle, S. LaPlaca, J. Appl. Phys. 51 (1980) 373–382.
[18] Z. Balogh Ibrahim, P. Stender, R. Schlesiger, G.-H. Greiwe, G. Schmitz, B. Parditka, G.A. Langer, A. Csik, Z. Erdélyi, Acta Mater. 76 (2014) 306–313.
[19] M. Ibrahim, Z. Balogh-Michels, P. Stender, D. Baither, G. Schmitz, Acta Mater. 112 (2016) 315–325.
[20] I. Souli, V.L. Terzisyska, J. Keckes, W. Robl, J. Zechner, C. Mitterer, J. Vac. Sci. Technol. B 35 (2017), 022201.
[21] S. Coffa, J.M. Poate, D.C. Jacobson, W. Frank, D. Gustin, Phys. Rev. B 45 (1992) 8355–8358.
[22] E.R. Weber, Appl. Phys. A Mater. Sci. Process. 30 (1983) 1–22.
[23] T.C. Frank, J.L. Falconer, Appl. Surf. Sci. 14 (1982–1983) 359–374.
[24] A.M. Gusak, K.P. Gurov, Solid State Phenom. 23–24 (1992) 117–122.
[25] F. Hodaj, A.M. Gusak, Acta Mater. 52 (2004) 4305–4315.
[26] R.R. Chromik, W.K. Neils, E.J. Cotts, J. Appl. Phys. 86 (1999) 4273–4281.
[27] T.B. Massalski (Ed.), Binary Alloys Phase Diagrams, ASM International, Materials Park, OH, 1992.
[28] D. Shin, J.E. Saal, Z.K. Liu, Calphad 32 (2008) 520–526.
[29] A.T. Dinsdale, Calphad 15 (1991) 317–425.
[30] J.C.C. Fan, C.H. Anderson Jr, J. Appl. Phys. 52 (1981) 4003–4006.
[31] M. Fugger, M. Plappert, C. Schäffer, O. Humbel, H. Hutter, H. Danninger, M. Nowottnick, Microelectron. Reliab. 54 (2014) 2487–2493.
[32] S.B. Lee, D.K. Choi, F. Phillipp, K.S. Jeon, C.K. Kim, Appl. Phys. Lett. 88 (2006), 083117.
[33] M. Au, Y. He, Y. Zhao, H. Ghassemi, R.S. Yassar, B. Garcia-Diaz, T. Adams, J. Power Sources 196 (2011) 9640–9647.
[34] G. Molnár, G. Erdélyi, G.A. Langer, D.L. Beke, A. Csik, G.L. Katona, L. Daróczi, M. Kis-Varga, A. Dudás, Vacuum 98 (2013) 70–74.
[35] A. Lakatos, G.A. Langer, A. Csik, C. Cserhati, M. Kis-Varga, L. Daroczi, G.L. Katona, Z. Erdélyi, G. Erdélyi, K. Vad, D.L. Beke, Appl. Phys. Lett. 97 (2010), 233103.
[36] U. Gösele, K.N. Tu, J. Appl. Phys. 53 (1982) 3252–3260.
[37] B.E. Deal, A.S. Grove, J. Appl. Phys. 36 (1965) 3770–3778.
[38] J.J. Tomán, G. Schmitz, Z. Erdélyi, Comput. Mater. Sci. 138 (2017) 183–191.